



ELSEVIER

Available online at www.sciencedirect.com



Nuclear Physics B Proceedings Supplement 00 (2021) 1–7

**Nuclear Physics B
Proceedings
Supplement**

Measurement of the total cross section from elastic scattering in pp collisions at $\sqrt{s} = 7$ TeV with the ATLAS detector

Hasko Stenzel

On behalf of the ATLAS Collaboration

Justus-Liebig Universität Gießen, II. Physikalisches Institut, Heinrich-Buff Ring 16, D-35392 Giessen, Germany

Abstract

In this contribution a measurement of the total pp cross section with the ATLAS detector at the LHC at $\sqrt{s} = 7$ TeV is presented. In a special run with high- β^* beam optics, the differential elastic cross section is measured as a function of the Mandelstam momentum transfer variable t . The measurement is performed with the ALFA sub-detector of ATLAS. Using a fit to the differential elastic cross section in the $|t|$ range from 0.01 GeV^2 to 0.1 GeV^2 to extrapolate to $|t| \rightarrow 0$, the total cross section, $\sigma_{\text{tot}}(pp \rightarrow X)$, is measured via the optical theorem to be:

$$\sigma_{\text{tot}}(pp \rightarrow X) = 95.35 \pm 0.38 \text{ (stat.)} \pm 1.25 \text{ (exp.)} \pm 0.37 \text{ (extr.) mb} ,$$

where the first error is statistical, the second accounts for all experimental systematic uncertainties and the last is related to uncertainties in the extrapolation to $|t| \rightarrow 0$. In addition, the slope of the elastic cross section at small $|t|$ is determined to be $B = 19.73 \pm 0.14 \text{ (stat.)} \pm 0.26 \text{ (syst.) GeV}^{-2}$.

Keywords: Elastic scattering, total cross section

1. Introduction

The total cross section is a fundamental parameter of strong interactions, setting the scale for the interaction strength for all processes at a given energy. A calculation of the total cross section from first principles, based upon quantum chromodynamics (QCD), is not possible, since large distances are involved. A measurement of the total cross section can still be performed via elastic scattering by using the optical theorem, which relates the imaginary part of the forward elastic-scattering amplitude to the total cross section:

$$\sigma_{\text{tot}} \propto \text{Im} [f_{\text{el}}(t \rightarrow 0)] , \quad (1)$$

where $f_{\text{el}}(t \rightarrow 0)$ is the elastic-scattering amplitude extrapolated to the forward direction, i.e. at $|t| \rightarrow 0$, t being the four-momentum transfer. In this analysis, a luminosity-dependent method is used to extract the total cross section from a fit to the differential elastic cross

section according to

$$\sigma_{\text{tot}}^2 = \frac{16\pi(\hbar c)^2}{1 + \rho^2} \left. \frac{d\sigma_{\text{el}}}{dt} \right|_{t \rightarrow 0} , \quad (2)$$

where ρ represents a small correction arising from the ratio of the real to imaginary part of the elastic-scattering amplitude in the forward direction and is taken from theory.

More details on the results presented in this paper are given in Ref. [1]. The quantities measured and reported here have also been measured at the LHC by the TOTEM experiment [2, 3].

2. Experimental setup

ATLAS is a multi-purpose detector designed to study elementary processes in proton–proton interactions at

arXiv:1409.3704v1 [hep-ex] 12 Sep 2014

the TeV energy scale. A detailed description of the ATLAS detector can be found in Ref. [4]. Elastic scattering protons are detected with the ALFA (Absolute Luminosity For ATLAS) Roman Pot detector system. Two tracking stations are placed on each side of the central ATLAS detector at distances of 238 m and 241 m from the interaction point. The detectors are housed in so-called Roman Pots (RPs) which can be moved vertically close to the circulating proton beams. The RPs are instrumented with main tracking detectors (MDs) to determine the track coordinates, with overlap detectors (ODs) to determine the distance between the upper and lower detectors, each set of these detectors is supplemented by trigger scintillators. Each MD consists of 2 times 10 layers of 64 square scintillating fibres with 0.5 mm side length glued on titanium plates. The fibres on the front and back sides of each titanium plate are orthogonally arranged at angles of $\pm 45^\circ$ with respect to the y -axis. The overlap detectors consist of three layers of 30 scintillating fibres per layer measuring the vertical coordinate of traversing beam-halo particles or shower fragments. The station and detector naming scheme is depicted in Fig. 1. The stations A7R1 and B7R1 are positioned at $z = -237.4$ m and $z = -241.5$ m respectively in the outgoing beam 1 (C side), while the stations A7L1 and B7L1 are situated symmetrically in the outgoing beam 2 (A side).

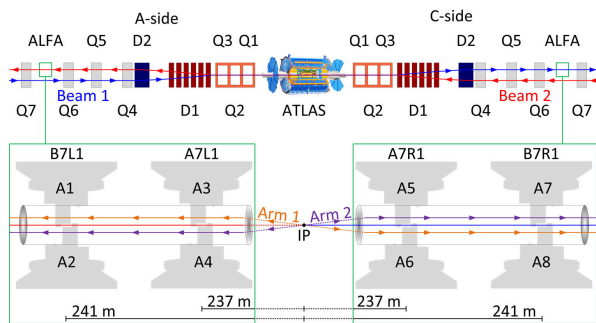


Figure 1: A sketch of the experimental set-up, not to scale, showing the positions of the ALFA Roman Pot stations in the outgoing LHC beams, and the quadrupole (Q1–Q6) and dipole (D1–D2) magnets situated between the interaction point and ALFA. The ALFA detectors are numbered A1–A8, and are combined into inner stations A7R1 and A7L1, which are closer to the interaction point, and outer stations B7R1 and B7L1.

The data were recorded in a dedicated low-luminosity run using beam optics with a β^* of 90 m; details of the beam optics settings can be found in Refs. [5, 6]. For elastic-scattering events, the main pair of colliding bunches was used, which contained around 7×10^{10} protons per bunch. Very precise positioning of the RPs is

mandatory to achieve the desired precision on the position measurement of 20–30 μm in both the horizontal and vertical dimensions. The first step is a beam-based alignment procedure to determine the position of the RPs with respect to the proton beams. In a second step the detector positions are directly determined from the elastic-scattering data. The alignment procedure is based on the distribution of track positions in the RP stations in the full elastic-scattering event sample. This distribution forms a narrow ellipse with its major axis in the vertical (y) direction, with an aperture gap between the upper and lower detectors. The measured distances between upper and lower MDs and the rotation symmetry of scattering angles are used as additional constraints. Three parameters are necessary to align each MD: the horizontal and vertical positions and the rotation angle around the beam axis. The horizontal detector positions and the rotation angles are determined from a fit of a straight line to a profile histogram of the narrow track patterns in the upper and lower MDs. The uncertainties are 1–2 μm for the horizontal coordinate and 0.5 mrad for the angles. For the vertical detector positioning, the essential input is the distance between the upper and lower MDs. The achieved precision on the vertical alignment is about 80 μm .

To trigger on elastic-scattering events, two main triggers were used. The triggers required a coincidence of the main detector trigger scintillators between either of the two upper (lower) detectors on side A and either of the two lower (upper) detectors on side C. The trigger efficiency for elastic-scattering events was determined from a data stream in which all events with a hit in any one of the ALFA trigger counters were recorded. In the geometrical acceptance of the detectors, the efficiency of the trigger used to record elastic-scattering events is $99.96 \pm 0.01\%$.

3. Measurement principle and beam optics

The data were recorded with a beam optics of high β^* of 90 m resulting in a small divergence and providing parallel-to-point focusing in the vertical plane. In parallel-to-point beam optics the betatron oscillation has a phase advance Ψ of 90° between the interaction point and the RPs, such that all particles scattered at the same angle are focused at the same position at the detector, independent of their production vertex position. The four-momentum transfer t is calculated from the scattering angle θ^* ; in elastic scattering at high energies this is given by:

$$-t = (\theta^* \times p)^2, \quad (3)$$

where p is the nominal beam momentum of the LHC of 3.5 TeV and θ^* is measured from the proton trajectories in ALFA. The trajectory $(w(z), \theta_w(z))$, where $w = x, y$ is the transverse position with respect to the nominal orbit at a distance z from the interaction point and θ_w is the angle between w and z , is given by the transport matrix \mathbf{M} and the coordinates at the interaction point (w^*, θ_w^*) :

$$\begin{pmatrix} w(z) \\ \theta_w(z) \end{pmatrix} = \mathbf{M} \begin{pmatrix} w^* \\ \theta_w^* \end{pmatrix} = \begin{pmatrix} M_{11} & M_{12} \\ M_{21} & M_{22} \end{pmatrix} \begin{pmatrix} w^* \\ \theta_w^* \end{pmatrix}, \quad (4)$$

where the elements of the transport matrix can be calculated from the optical function β and its derivative with respect to z and Ψ . The t -reconstruction is based upon the track positions and certain transport matrix elements. The ALFA detector was designed to use the “subtraction” method to calculate the scattering angle:

$$\theta_w^* = \frac{w_A - w_C}{M_{12,A} + M_{12,C}}, \quad (5)$$

exploiting the fact that for elastic scattering the particles are back-to-back, the scattering angle at the A- and C-side are the same in magnitude and opposite in sign, and the protons originate from the same vertex. Three different alternative methods “local subtraction”, “lattice” and “local angle” [1] using a combination of the track position and angle between inner and outer stations and different sets of matrix elements are used to derive constraints on the beam optics and as a cross-check for the nominal subtraction method. For all methods t is calculated from the scattering angles as follows:

$$-t = ((\theta_x^*)^2 + (\theta_y^*)^2) p^2. \quad (6)$$

The precision of the t -reconstruction depends on knowledge of the elements of the transport matrix. From the design of the 90 m beam optics along with the alignment parameters of the magnets, the magnet currents and the field calibrations, all transport matrix elements can be calculated. This initial set of matrix elements is referred to as “design optics”. Small corrections, allowed within the range of the systematic uncertainties, need to be applied to the design optics for the measurement of σ_{tot} . Constraints on beam optics parameters are derived from the ALFA data, exploiting the fact that the reconstructed scattering angle must be the same for different reconstruction methods using different transport matrix elements. Two classes of constraints are distinguished:

- Correlations between positions or angles measured either at the A-side and C-side or at inner and outer

stations of ALFA. These are used to infer the ratio of matrix elements in the beam transport matrix. The resulting constraints are independent of any optics input.

- Correlations between the reconstructed scattering angles. These are calculated using different methods to derive further constraints on matrix elements as scaling factors. These factors indicate the amount of scaling needed to be applied to a given matrix element ratio in order to equalize the measurement of the scattering angle. These constraints depend on the given optics model. The design beam optics with quadrupole currents measured during the run is used as reference to calculate the constraints.

The best example is the comparison of the scattering angle in the horizontal plane reconstructed with the subtraction method, which is based on the position and $M_{12,x}$, and with the local angle method, which is based on the local angle and $M_{22,x}$. The scaling factor for the matrix element ratio M_{12}/M_{22} is derived from the slope of the difference of the scattering angle obtained with the two methods as a function of the scattering angle determined with the subtraction method, as shown in Fig. 2. In total 14 constraints are derived from ALFA data.

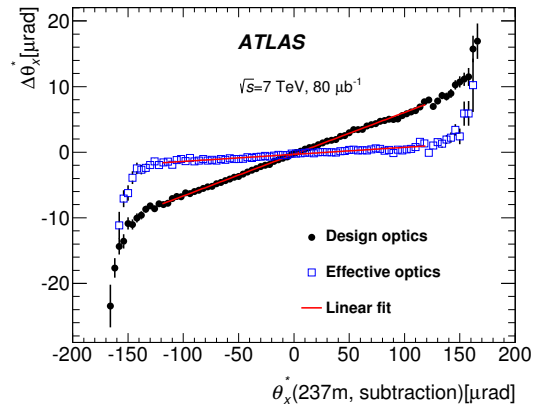


Figure 2: The difference in reconstructed scattering angle $\Delta\theta_x^*$ between the subtraction and local angle methods as a function of the scattering angle from subtraction method for the inner detectors. The line represents the result of a linear fit. Values obtained using the tuned effective optics are also shown for comparison.

The constraints are combined in a fit used to determine the beam optics. The free parameters of the fit are the quadrupole strengths in both beams. The chosen configuration, called the effective optics, is one solution

among many. This solution is obtained by allowing only the inner triplet magnets Q1 and Q3 to vary coherently from their nominal strength. Q1 and Q3 were manufactured at a different site from the other quadrupoles, and relative calibration differences are possible. The fit resulted in an offset of approximately 0.3% for the strength of Q1 and Q3, with a difference of about 10% between the two beams and the uncertainty from the fit is also of 10%. The χ^2 of the fit includes the systematic uncertainties of the constraints and is of good quality with $\chi^2/N_{\text{dof}} = 1.1$. This effective optics is used for the total cross-section measurement.

4. Data Analysis

Events are required to pass the trigger conditions for elastic-scattering events, and have a reconstructed track in all four detectors of the arm which fired the trigger. Events with additional tracks in detectors of the other arm arise from the overlap of halo protons with elastic-scattering protons and are retained. Further geometrical cuts on the left-right acollinearity are applied, exploiting the back-to-back topology of elastic-scattering events. The position difference between the left and the right sides is required to be within 3.5σ of its resolution determined from simulation. An efficient cut against non-elastic background is obtained from the correlation of the local angle between two stations and the position in the horizontal plane. Finally, fiducial cuts to ensure a good containment inside the detection area are applied to the vertical coordinate. It is required to be at least $60 \mu\text{m}$ from the edge of the detector nearer the beam, where the full detection efficiency is reached. At large vertical distance, the vertical coordinate must be at least 1 mm away from the shadow of the beam screen, a protection element of the quadrupoles, in order to minimize the impact from showers generated in the beam screen. At the end of the selection procedure 805,428 events survive all cuts.

A small fraction of background events is expected to survive the elastic event selection cuts. The background events peak at small values of x and y and thus constitute an irreducible background at small t . The background predominantly originates from accidental coincidences of beam-halo particles, but single diffractive protons in coincidence with a halo proton at the opposite side may also contribute. The irreducible background fraction is estimated by counting events in the “anti-golden” topology with two tracks in both upper or both lower detectors [1], which also allows constructing the t -spectrum and subtracting it from the spectrum of the selected sample. The background contamination is

about 0.5% with large systematic uncertainties of 50–80%, which are dominated by the background normalization uncertainty.

Elastic-scattering events inside the acceptance region are expected to have a proton track in each of the four detectors of the corresponding spectrometer arm. Losses of elastic events occur in the case of interactions of the protons with the stations or detectors, which result in too large fibre hit multiplicities and a failure of the track reconstruction algorithm. The event reconstruction efficiency is used to correct for these losses and its determination is based on a tag-and-probe approach using a data-driven method. Elastic events not fully reconstructed and thus not used for the analysis are grouped into several reconstruction cases, according to the number of detectors with a reconstructed track out of the four detectors ideally present. The reconstruction efficiency is given by:

$$\varepsilon_{\text{rec}} = \frac{N_{4/4}}{N_{4/4} + N_{3/4} + N_{2/4} + N_{1+1/4} + N_{1/4} + N_{0/4}}, \quad (7)$$

where $N_{k/4}$ is the number of events with k detectors with at least one reconstructed track in a spectrometer arm and $N_{1+1/4}$ is the number of events with a track reconstructed in only one detector at each side. The event reconstruction efficiencies in arm 1 and arm 2 are determined to be $\varepsilon_{\text{rec},1} = 0.8974 \pm 0.0004$ (stat.) ± 0.0061 (syst.) and $\varepsilon_{\text{rec},2} = 0.8800 \pm 0.0005$ (stat.) ± 0.0092 (syst.) respectively.

ATLAS exploits several detectors and algorithms to determine the luminosity and evaluate the related systematic uncertainty [7]. The absolute luminosity scale of each algorithm was calibrated [7] by the van der Meer (*vdM*) method [8] in an intermediate luminosity regime ($L \sim 5 \times 10^{30} \text{ cm}^{-2} \text{ s}^{-1}$).

The conditions in the low-luminosity run analysed here are very different from those in high-luminosity runs. The instantaneous luminosity is about six orders of magnitude lower ($L \sim 5 \times 10^{27} \text{ cm}^{-2} \text{ s}^{-1}$), the beam-gas contribution, normally negligible, can become competitive with the collision rate, but the background due to slowly decaying, collision-induced radiation (often called “afterglow” [7]) becomes conversely less important. The luminosity is determined using the BCM (beam conditions monitor), as in Ref. [7], and other detectors and algorithms are used to assess the systematic uncertainty. The integrated luminosity for the selected running period is:

$$L_{\text{int}} = 78.7 \pm 0.1 \text{ (stat.)} \pm 1.9 \text{ (syst.) } \mu\text{b}^{-1},$$

and the total systematic uncertainty amounts to 2.3%, which comprises the scale uncertainty, the overall

calibration-transfer uncertainty and the background uncertainty.

Simulations for the calculation of the acceptance corrections are carried out with PYTHIA8 [9, 10]. Generated particles are transported from the interaction point to the RPs using either the transport matrix Eq. (4) or the MadX [11] beam optics calculation package. A fast parameterization of the detector response is used for the detector simulation with the detector resolution tuned to the measured resolution. The measured t -spectrum in each arm, after background subtraction, is corrected for migration effects using an iterative, dynamically stabilised unfolding method [12]. A data-driven closure test is used to evaluate any bias in the unfolded data spectrum shape due to mis-modelling of the reconstruction-level spectrum shape in the simulation.

5. Results

In order to calculate the differential elastic cross section, several corrections are applied. The corrections are done individually per detector arm and the corrected spectra from the two arms are combined. In a given bin t_i , the cross section is calculated according to the following formula:

$$\frac{d\sigma}{dt_i} = \frac{1}{\Delta t_i} \times \frac{\mathcal{M}^{-1}[N_i - B_i]}{A_i \times \epsilon^{\text{reco}} \times \epsilon^{\text{trig}} \times \epsilon^{\text{DAQ}} \times L_{\text{int}}} , \quad (8)$$

where Δt_i is the bin width, \mathcal{M}^{-1} represents the unfolding procedure applied to the background-subtracted number of events $N_i - B_i$, A_i is the acceptance, ϵ^{reco} is the event reconstruction efficiency, ϵ^{trig} is the trigger efficiency, ϵ^{DAQ} is the dead-time correction and L_{int} is the integrated luminosity used for this analysis. The following uncertainties are propagated to the differential elastic cross section:

- The amount of background is varied by the difference between the yields obtained from different methods and different background shapes obtained from variations of the anti-golden method.
- The impact of alignment uncertainties is estimated from different sets of the alignment parameter values.
- The uncertainties related to the effective optics are obtained by varying the optics constraints, changing the strength and alignment of the quadrupoles, propagating the fit uncertainties to the resulting optics and varying beam transport parameters.

- The nuclear slope used in the simulation is varied conservatively by $\pm 1 \text{ GeV}^{-2}$ around 19.5 GeV^{-2} .
- Variations of the model for the detector parameterization in the simulation.
- Variations of the emittance used to calculate the angular divergence in the simulation.
- The event reconstruction efficiency is varied by its uncertainty.
- Variations of the track reconstruction parameters.
- The intrinsic unfolding uncertainty is determined from the data-driven closure test.
- The impact of a residual beam crossing angle in the horizontal plane of $\pm 10 \mu\text{rad}$ is taken into account. This variation is derived from the precision of the beam position monitors.
- The nominal beam energy used in the t -reconstruction is changed by 0.65% [13].
- The luminosity uncertainty of 2.3% is propagated to the cross section.

The total cross section and the slope parameter B are obtained from a fit of the theoretical spectrum

$$\begin{aligned} \frac{d\sigma}{dt} &= \frac{4\pi\alpha^2(\hbar c)^2}{|t|^2} \times G^4(t) \\ &- \sigma_{\text{tot}} \times \frac{\alpha G^2(t)}{|t|} [\sin(\alpha\phi(t)) + \rho \cos(\alpha\phi(t))] \\ &\times \exp\left(\frac{-B|t|}{2}\right) \\ &+ \sigma_{\text{tot}}^2 \frac{1 + \rho^2}{16\pi(\hbar c)^2} \times \exp(-B|t|) , \end{aligned} \quad (9)$$

where G is the electric form factor of the proton [14], ϕ is the Coulomb phase [15, 16] and the value of $\rho = 0.140 \pm 0.008$ is taken from Ref. [17]. Both the statistical and systematic uncertainties as well as their correlations are taken into account in the fit, shown in Fig. 3, which uses a profile minimization procedure [18]. Additional uncertainties arise from the extrapolation $|t| \rightarrow 0$. These are estimated from a variation of the upper end of the fit range from $-t = 0.1 \text{ GeV}^2$ to $-t = 0.15 \text{ GeV}^2$ [19]. The upper fit-range edge is also decreased by the same number of bins (six) to $|t| = 0.059 \text{ GeV}^2$ and the symmetrized change is adopted as a systematic uncertainty. Further uncertainties comprise the variation of ρ by its uncertainty and variations of the electric form factor and Coulomb phase [1]. The results including uncertainties

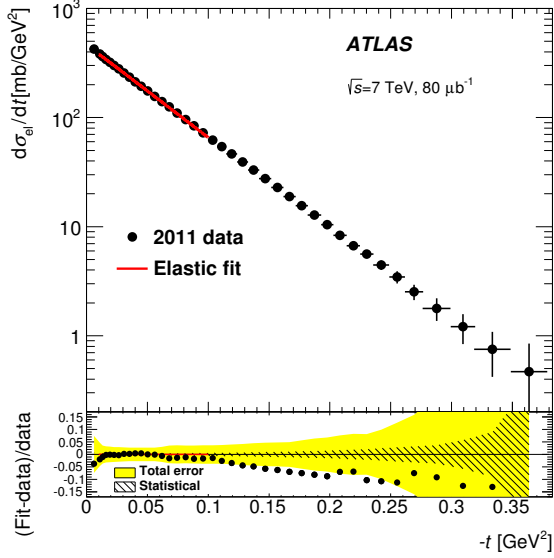


Figure 3: A fit of the theoretical prediction with σ_{tot} and B as free parameters to the differential elastic cross section reconstructed with the subtraction method. In the lower panel the points represent the normalized difference between fit and data, the yellow area represents the total experimental uncertainty and the hatched area the statistical component. The red line indicates the fit range.

	σ_{tot} [mb]	B [GeV^{-2}]
Central result	95.35	19.73
Statistical error	0.38	0.14
Experimental error	1.25	0.19
Extrapolation error	0.37	0.17
Total error	1.36	0.35

Table 1: Results for the total cross section and nuclear slope.

are summarized in Table 1. Several cross-checks of the analysis were carried out, including the investigation of the four different t -reconstruction algorithms, replacing the profile fit with a simple χ^2 -minimization using statistical uncertainties only, analyzing the total cross section separately in each arm of ALFA, replacing the unfolding procedure of the data by a method where all corrections are applied to the theoretical prediction, which is then fit to raw data and finally the full sample was split into several time-ordered sub-samples to investigate a potential time dependence. All cross-checks gave consistent results. Additionally, different theoretical predictions including possible non-exponential terms in the nuclear amplitude were used to extract the total cross section and the scatter of results was found consistent with the extrapolation uncertainty [1].

From the fitted parameterization of the differential elastic cross section several additional quantities can be derived. The total elastic cross section is obtained from the nuclear scattering term, whereas the Coulomb and interference terms are not taken into account:

$$\begin{aligned} \sigma_{\text{el}} &= \int_{t=0}^{t=\infty} \sigma_{\text{tot}}^2 \frac{1+\rho^2}{16\pi(\hbar c)^2} \exp(-B|t|) dt \quad (10) \\ &= \frac{\sigma_{\text{tot}}^2}{B} \frac{1+\rho^2}{16\pi(\hbar c)^2} . \end{aligned}$$

The differential cross section at the optical point, $|t| \rightarrow 0$, derived from the total cross-section fit, is $d\sigma_{\text{el}}/dt|_{t \rightarrow 0} = 474 \pm 4$ (stat.) ± 13 (syst.) mb/GeV^2 , where the systematic uncertainty includes all experimental and extrapolation uncertainties. Integrating the parameterized form of the differential cross section over the full t -range yields the total elastic cross section:

$$\sigma_{\text{el}} = 24.00 \pm 0.19 \text{ (stat.)} \pm 0.57 \text{ (syst.) mb.}$$

The measured integrated elastic cross section in the fiducial range from $-t = 0.0025 \text{ GeV}^2$ to $-t = 0.38 \text{ GeV}^2$ corresponds to 90% of the total elastic cross section:

$$\sigma_{\text{el}}^{\text{observed}} = 21.66 \pm 0.02 \text{ (stat.)} \pm 0.58 \text{ (syst.) mb.}$$

The total elastic cross section is used to determine the total inelastic cross section by subtraction from the total cross section. The resulting value is:

$$\sigma_{\text{inel}} = 71.34 \pm 0.36 \text{ (stat.)} \pm 0.83 \text{ (syst.) mb.}$$

6. Discussion

The result for the total hadronic cross section presented here, $\sigma_{\text{tot}} = 95.35 \pm 1.36 \text{ mb}$, can be compared to the value measured by TOTEM in the same LHC fill using a luminosity-dependent analysis, $\sigma_{\text{tot}} = 98.6 \pm 2.2 \text{ mb}$ [20]. Assuming the uncertainties are uncorrelated, the difference between the ATLAS and TOTEM values corresponds to 1.3σ . The uncertainty on the TOTEM result is dominated by the luminosity uncertainty of $\pm 4\%$, while the measurement reported here profits from a smaller luminosity uncertainty of only $\pm 2.3\%$. The value of the nuclear slope parameter $B = 19.73 \pm 0.29 \text{ GeV}^{-2}$ is in good agreement with the TOTEM measurement of $19.89 \pm 0.27 \text{ GeV}^{-2}$ [20]. These large values of the B -parameter confirm that elastically scattered protons continue to be confined to a gradually narrowing cone. The elastic cross section is measured to be $24.0 \pm 0.6 \text{ mb}$. This is in agreement with

the TOTEM result of 25.4 ± 1.1 mb within 1.1σ . The ratio of the elastic cross section to the total cross section is often taken as a measure of the opacity of the proton. Measurements shed light on whether the black disc limit of a ratio of 0.5 is being approached. The TOTEM value is $\sigma_{\text{el}}/\sigma_{\text{tot}} = 0.257 \pm 0.005$ [3, 21], while the measurement reported here gives $\sigma_{\text{el}}/\sigma_{\text{tot}} = 0.252 \pm 0.004$. All derived measurements depend on σ_{tot} and B and are therefore highly correlated.

7. Conclusion

In this paper a measurement of the elastic pp cross section and the determination of the total cross section using the optical theorem at $\sqrt{s} = 7$ TeV by the ATLAS experiment at the LHC with the ALFA sub-detector is presented. The data were recorded in 2011 during a special run with high- β^* optics, where an integrated luminosity of $80 \mu\text{b}^{-1}$ was accumulated. The analysis uses data-driven methods to determine relevant beam optics parameters, event reconstruction efficiency and to tune the simulation. A key element of this analysis is the determination of the effective beam optics, which takes into account measurements from ALFA that are sensitive to ratios of transport matrix elements and calibration uncertainties of the quadrupoles. A detailed evaluation of the associated systematic uncertainties includes the comparison of different t -reconstruction methods that are sensitive to different transport matrix elements. A dedicated effort was made to determine the absolute luminosity for this run while taking into account the special conditions with a very low number of interactions per bunch crossing. From a fit to the differential elastic cross section, using the optical theorem, the total cross section is determined to be:

$$\sigma_{\text{tot}}(pp \rightarrow X) = 95.35 \pm 1.36 \text{ mb} ,$$

where the total error includes statistical, experimental systematic and extrapolation uncertainties. The experimental systematic uncertainty is dominated by the uncertainty on the luminosity and on the nominal beam energy. In addition, the slope of the elastic differential cross section at small t was determined to be:

$$B = 19.73 \pm 0.35 \text{ GeV}^{-2} .$$

More elastic data were recorded at $\sqrt{s} = 8$ TeV with a high- β^* optics of 90 m and 1 km, which will allow probing the Coulomb-nuclear interference regime at yet smaller values of t . Additionally, during the shut-down of the LHC a substantial consolidation program was carried out to improve the performance of the ALFA detector in run 2 of the LHC.

References

- [1] ATLAS Collaboration, Measurement of the total cross section from elastic scattering in pp collisions at $\sqrt{s} = 7$ TeV with the ATLAS detector, submitted to Nucl. Phys. B. [arXiv:1408.5778](#).
- [2] G. Antchev, et al. (TOTEM Collaboration), Double diffractive cross-section measurement in the forward region at LHC, Phys. Rev. Lett. 111 (2013) 012001. [arXiv:1308.6722](#).
- [3] G. Antchev, et al. (TOTEM Collaboration), Luminosity-independent measurements of total, elastic and inelastic cross-sections at $\sqrt{s} = 7$ TeV, Europhys. Lett. 101 (2013) 21004.
- [4] ATLAS Collaboration, The ATLAS Experiment at the CERN Large Hadron Collider, JINST 3 (2008) S08003.
- [5] H. Burkhardt, et al., 90m Optics Studies and Operation in the LHC, Conf. Proc. C1205201 (2012) 130.
- [6] H. Burkhardt, S. Cavalier, P. Puzo, A. Peskov, 90 m Beta* Optics for ATLAS/ALFA, Conf. Proc. C110904 (2011) 1798.
- [7] ATLAS Collaboration, Improved luminosity determination in pp collisions at $\sqrt{s} = 7$ TeV using the ATLAS detector at the LHC, Eur. Phys. J. C 73 (2013) 2518. [arXiv:1302.4393](#).
- [8] S. van der Meer, Calibration of the effective beam height in the ISR, ISR-PO-68-31 (1968) <http://cds.cern.ch/record/296752>.
- [9] T. Sjöstrand, S. Mrenna, P. Skands, A Brief Introduction to PYTHIA 8.1, Comput. Phys. Commun. 178 (2008) 852. [arXiv:0710.3820](#).
- [10] T. Sjöstrand, S. Mrenna, P. Skands, PYTHIA 6.4 physics and manual, JHEP 0605 (2006) 026. [arXiv:hep-ph/0603175](#).
- [11] CERN Accelerator Beam Physics Group, Mad - methodical accelerator design, <http://mad.web.cern.ch/mad/> (2014).
- [12] B. Malaescu, An Iterative, Dynamically Stabilized (IDS) Method of Data Unfolding. [arXiv:1106.3107](#).
- [13] J. Wenninger, Energy Calibration of the LHC Beams at 4 TeV, CERN-ATS-2013-040, <http://cds.cern.ch/record/1546734> (2013).
- [14] R. N. Cahn, Coulombic-hadronic interference in an eikonal model, Z. Phys. C 15 (1982) 253.
- [15] H. A. Bethe, Scattering and polarization of protons by nuclei, Ann. Phys. 3 (1958) 190.
- [16] G. B. West, D. R. Yennie, Coulomb interference in high-energy scattering, Phys. Rev. 172 (1968) 1413.
- [17] J. Cudell, et al., Benchmarks for the Forward Observables at RHIC, the Tevatron Run II and the LHC, Phys. Rev. Lett. 89 (2002) 201801. [arXiv:hep-ph/0206172](#).
- [18] V. Blobel, Some Comments on χ^2 Minimization Applications, eConf C 030908 (2003) MOET002. <http://www.slac.stanford.edu/econf/C030908/proceedings.html>.
- [19] V. A. Khoze, A. D. Martin, M. G. Ryskin, Soft diffraction and the elastic slope at Tevatron and LHC energies: A multi-Pomeron approach, Eur. Phys. J. C 18 (2000) 167. [arXiv:hep-ph/0007359](#).
- [20] G. Antchev, et al. (TOTEM Collaboration), Measurement of proton-proton elastic scattering and total cross-section at $\sqrt{s} = 7$ TeV, Europhys. Lett. 101 (2013) 21002.
- [21] G. Antchev, et al. (TOTEM Collaboration), Measurement of proton-proton inelastic scattering cross-section at $\sqrt{s} = 7$ TeV, Europhys. Lett. 101 (2013) 21003.